

# Supplementary Materials: Evaluation of the Quality of NDVI3g Dataset against Collection 6 MODIS NDVI in Central Europe between 2000 and 2013

Anikó Kern Hrvoje Marjanović and Zoltán Barcza

## 1. Basic Statistics between the Different NDVI Datasets

**Table S1.** Relationship between the different NDVI datasets (NDVI3g with different processing levels versus MODIS) at the grid of the NDVI3g for the selected study area for the 2000–2013 and 2003–2013 periods based on two different resampled datasets. Bias represents the mean difference between NDVI3g and NDVI<sub>MODIS</sub>.

		Maximum NDVI Based MODIS				Reflectance Based MODIS			
		R <sup>2</sup>	RMSE	Bias	Mean Absolute Deviation	R <sup>2</sup>	RMSE	Bias	Mean Absolute Deviation
Terra (2000–2013)	Original NDVI3g	0.721	0.122	−0.008	0.095	0.739	0.125	0.046	0.101
	Bise-filtered NDVI3g	0.763	0.107	0.020	0.085	0.774	0.125	0.074	0.103
	Harmonized NDVI3g	0.954	0.034	−0.000	0.024	0.953	0.036	−0.000	0.027
Aqua (2003–2013)	Original NDVI3g	0.736	0.122	−0.010	0.095	0.747	0.126	0.045	0.102
	Bise-filtered NDVI3g	0.778	0.106	0.018	0.084	0.782	0.125	0.073	0.103
	Harmonized NDVI3g	0.966	0.029	−0.000	0.021	0.959	0.034	−0.000	0.025

**Table S2.** Relationship between the different Terra/MODIS and Aqua/MODIS NDVI datasets on the grid of the NDVI3g for the selected study area during the overlapping 2003–2013 period. Bias is defined as the mean difference between Terra/MODIS and Aqua/MODIS.

	Maximum NDVI Based Terra/MODIS (2003–2013)				Reflectance Based Terra/MODIS (2003–2013)			
	R <sup>2</sup>	Rmse	Bias	Mean Absolute Deviation	R <sup>2</sup>	Rmse	Bias	Mean Absolute Deviation
Maximum NDVI based Aqua/MODIS (2003–2013)	0.983	0.020	0.001	0.014	-	-	-	-
Reflectance based Aqua/MODIS (2003–2013)	-	-	-	-	0.974	0.027	0.002	0.018

## 2. Locations of the Selected Pixels with High Share of a Single Land Cover Type

**Table S3.** CORINE land class types.

LABEL1	LABEL2	LABEL3
1 Artificial surfaces	11 Urban fabric	111 Continuous urban fabric
		112 Discontinuous urban fabric
	12 Industrial, commercial and transport units	121 Industrial or commercial units
		122 Road and rail networks and associated land
		123 Port areas
13 Mine, dump and construction sites	124 Airports	
	131 Mineral extraction sites	
	132 Dump sites	
14 Artificial, non-agricultural vegetated areas	133 Construction sites	
	141 Green urban areas	
	142 Sport and leisure facilities	
2 Agricultural areas	21 Arable land	211 Non-irrigated arable land
		212 Permanently irrigated land
		213 Rice fields
	22 Permanent crops	221 Vineyards
		222 Fruit trees and berry plantations
		223 Olive groves
	23 Pastures	231 Pastures
24 Heterogeneous agricultural areas	241 Annual crops associated with permanent crops	

		242 Complex cultivation patterns
		243 Land principally occupied by agriculture, with significant areas of natural vegetation
		244 Agro-forestry areas
3 Forest and semi natural areas	31 Forests	311 Broad-leaved forest
		312 Coniferous forest
		313 Mixed forest
	32 Scrub and/or herbaceous vegetation associations	321 Natural grasslands
		322 Moors and heathland
		323 Sclerophyllous vegetation
33 Open spaces with little or no vegetation	324 Transitional woodland-shrub	
	331 Beaches, dunes, sands	
	332 Bare rocks	
	333 Sparsely vegetated areas	
	334 Burnt areas	
		335 Glaciers and perpetual snow
4 Wetlands	41 Inland wetlands	411 Inland marshes
		412 Peat bogs
	42 Maritime wetlands	421 Salt marshes
		422 Salines
		423 Intertidal flats
5 Water bodies	51 Inland waters	511 Water courses
		512 Water bodies
	52 Marine waters	521 Coastal lagoons
		522 Estuaries
		523 Sea and ocean

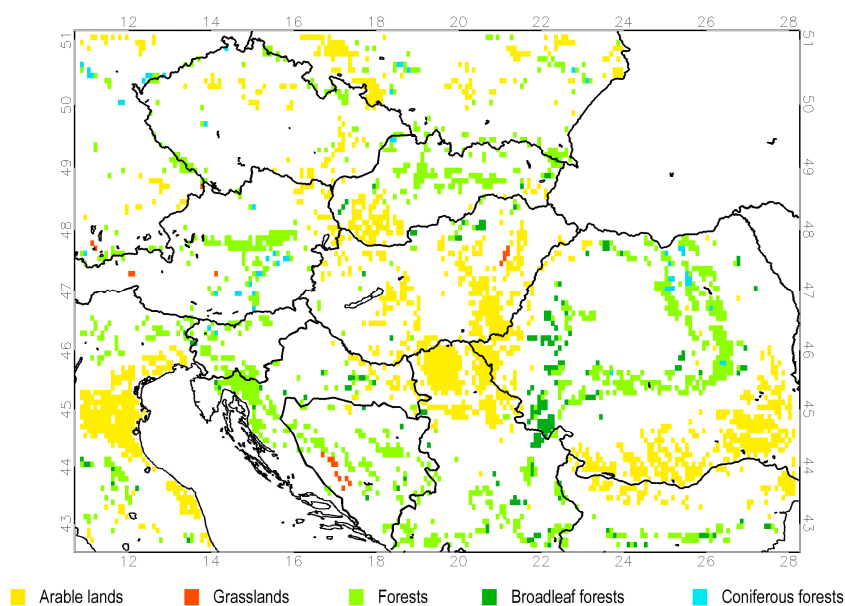


**Figure S1.** Location of the selected NDVI pixels at the grid of the NDVI3g dataset with a single land cover type share of minimum 80% for arable lands, forests, broadleaf forests and coniferous forests and with a minimum 70% share for grasslands. For more details see Section 2.8. *Land Cover Database* in the main paper.

### 3. Additional Maps and Figures Related to the Mean Seasonal Profile Comparison

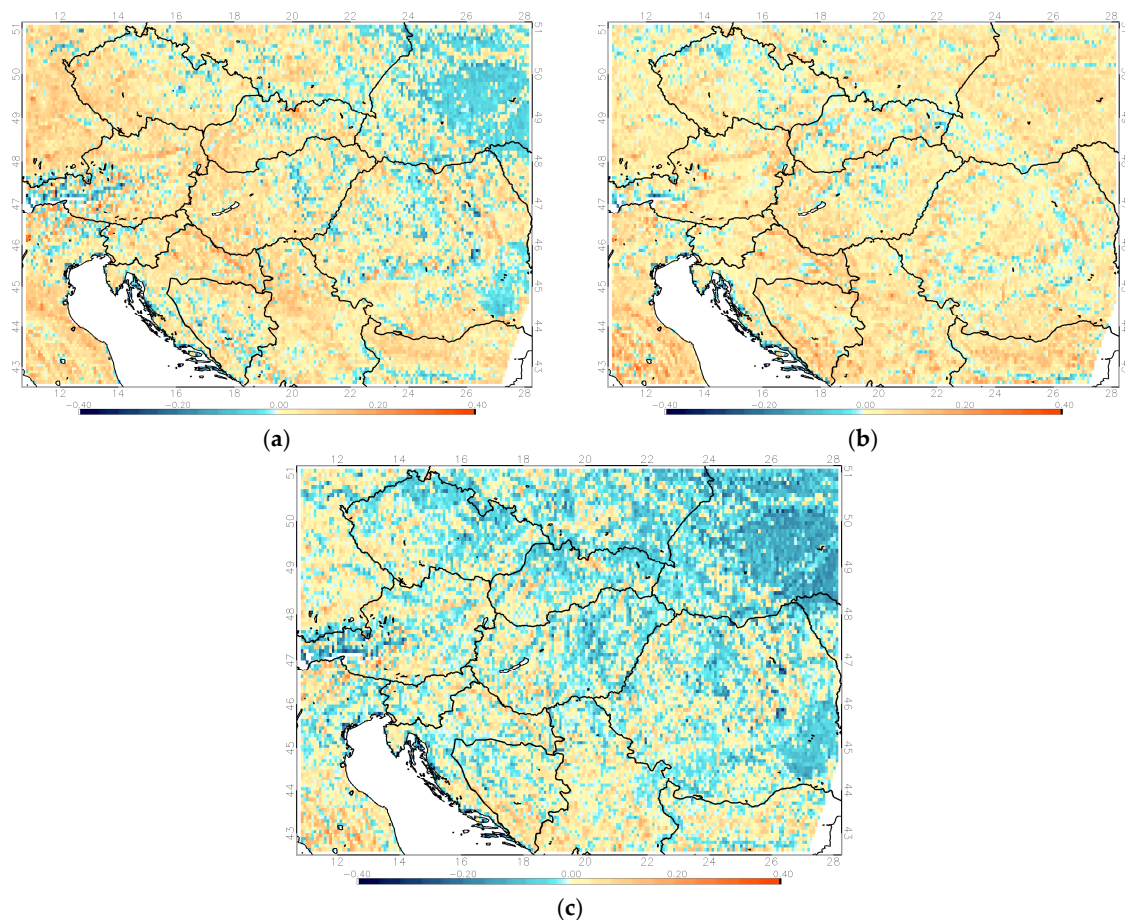


**Figure S2.** Seasonal bias maps between the NDVI values of the NDVI<sub>3go</sub> and the NDVI<sub>MODIS</sub> datasets during the overlapping 14 years calculated only for (a) spring, (b) summer and (c) autumn. Positive bias means higher NDVI<sub>3go</sub>.

### 4. Additional Maps and Figures Related to the SOS Comparison

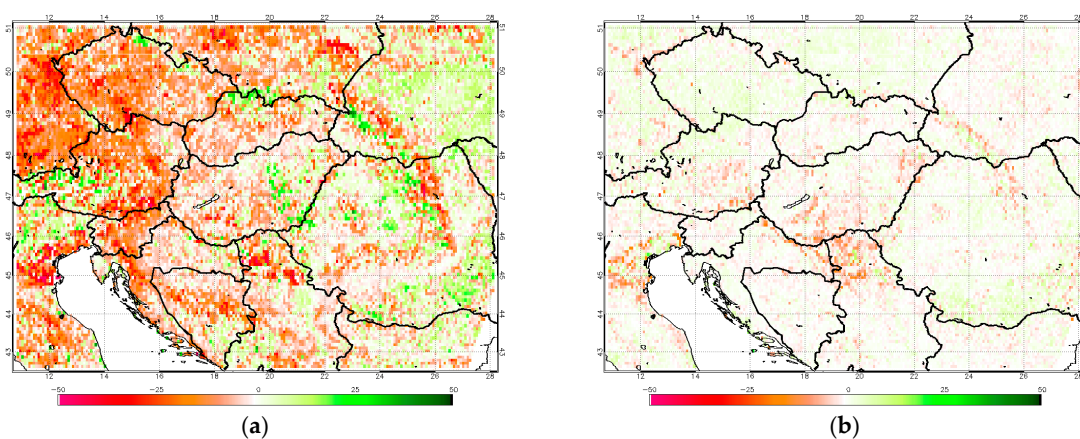


**Figure S3.** Maps of bias between the SOS derived from (a) NDVI<sub>3go</sub> and the Terra/NDVI<sub>MODIS</sub> datasets and (b) NDVI<sub>3gh</sub> and the Terra/NDVI<sub>MODIS</sub> dataset (expressed in days).

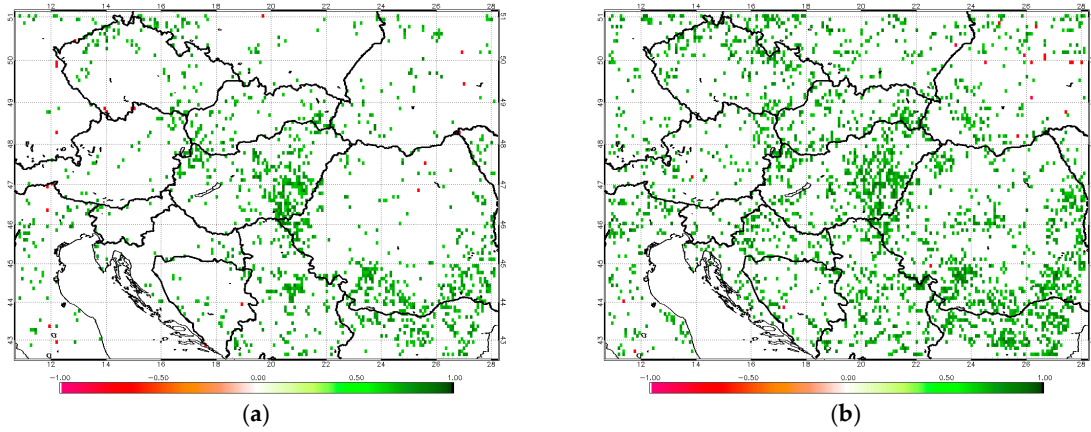


**Figure S4.** Maps of R between the SOS derived from (a) NDVI3go and the Terra/NDVIMODIS datasets and (b) NDVI3gh and the Terra/NDVIMODIS datasets, showing only the pixels with statistically significant R ( $p < 0.01$ ).

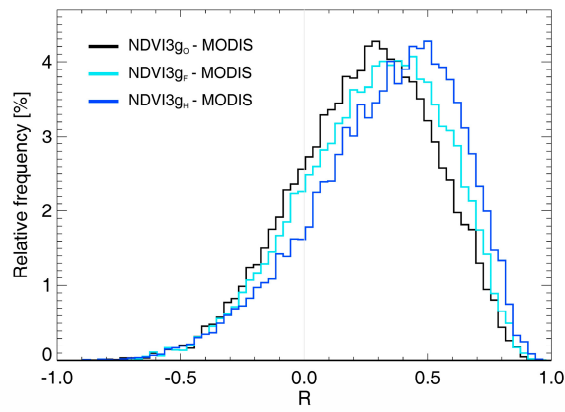


**Figure S5.** Frequency distribution of R values of SOS during the 2000–2013 time period for NDVI3go (black), NDVI3gf (light blue) and NDVI3gh (dark blue) datasets relative to the Terra NDVIMODIS dataset ( $n = 20191$ ).

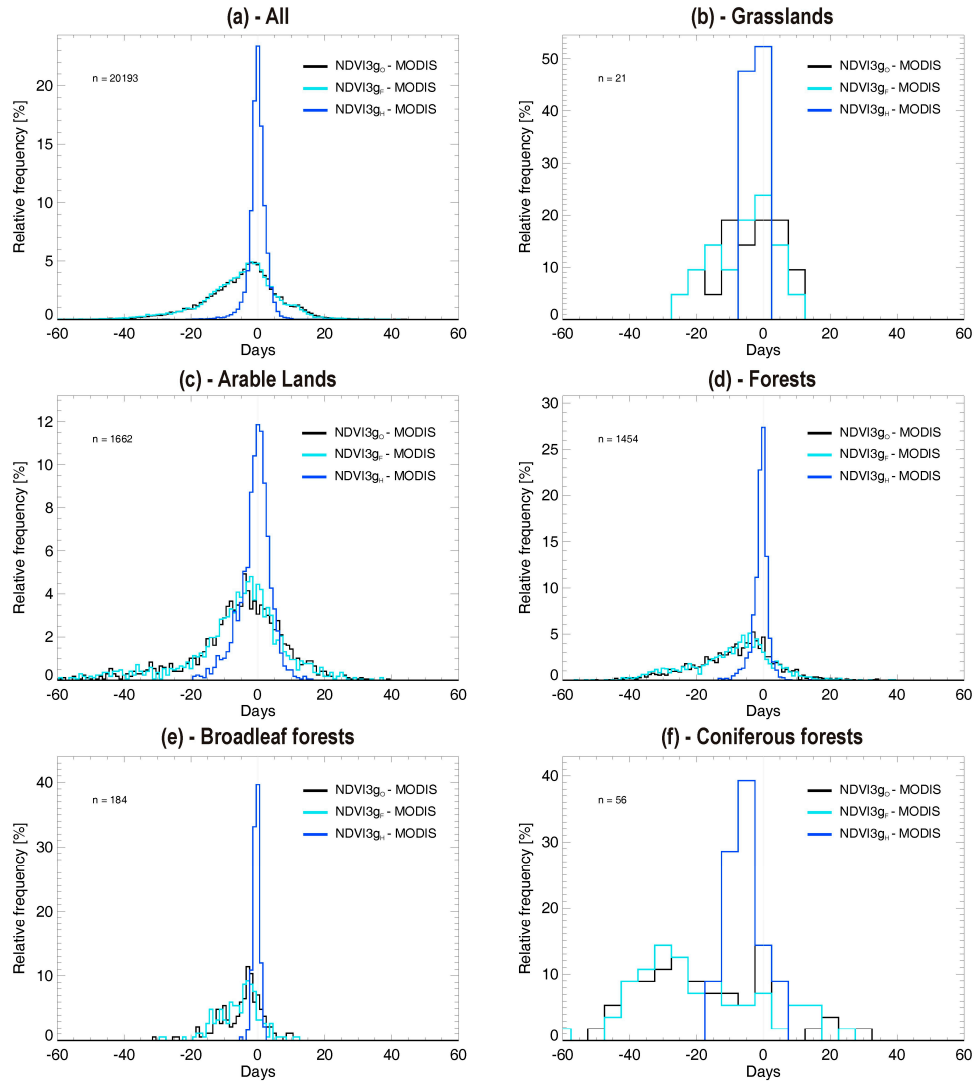


**Figure S6.** (a–f) Frequency distribution of SOS bias during the 2000–2013 time period for NDVI3g<sub>0</sub> (black), NDVI3g<sub>F</sub> (light blue) and NDVI3g<sub>H</sub> (dark blue) datasets relative to the Terra NDVI<sub>MODIS</sub> dataset for different land cover types. Positive bias means earlier SOS for MODIS.

**5. Additional Maps and Figures Related to the EOS Comparison**

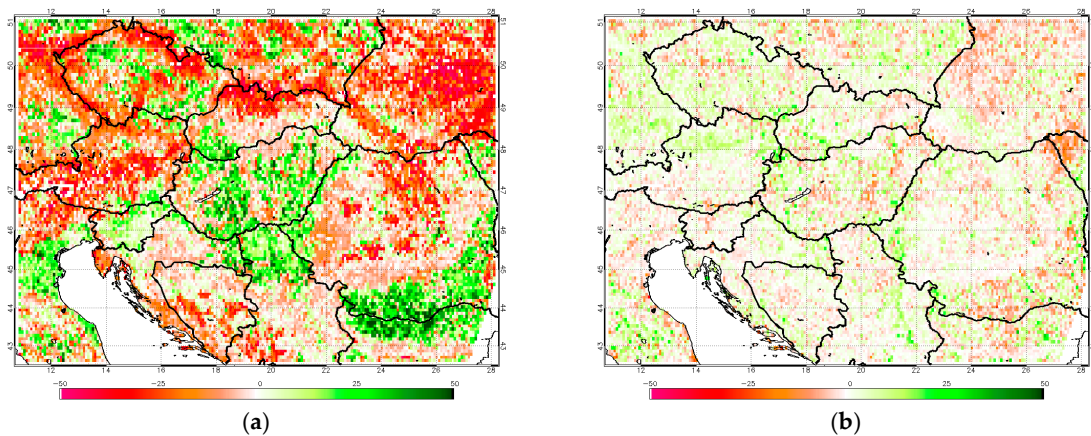


**Figure S7.** Maps of bias (expressed in days) between the EOS derived from (a) NDVI3g<sub>0</sub> and the Terra/NDVI<sub>MODIS</sub> datasets and (b) NDVI3g<sub>H</sub> and the Terra/NDVI<sub>MODIS</sub> dataset.

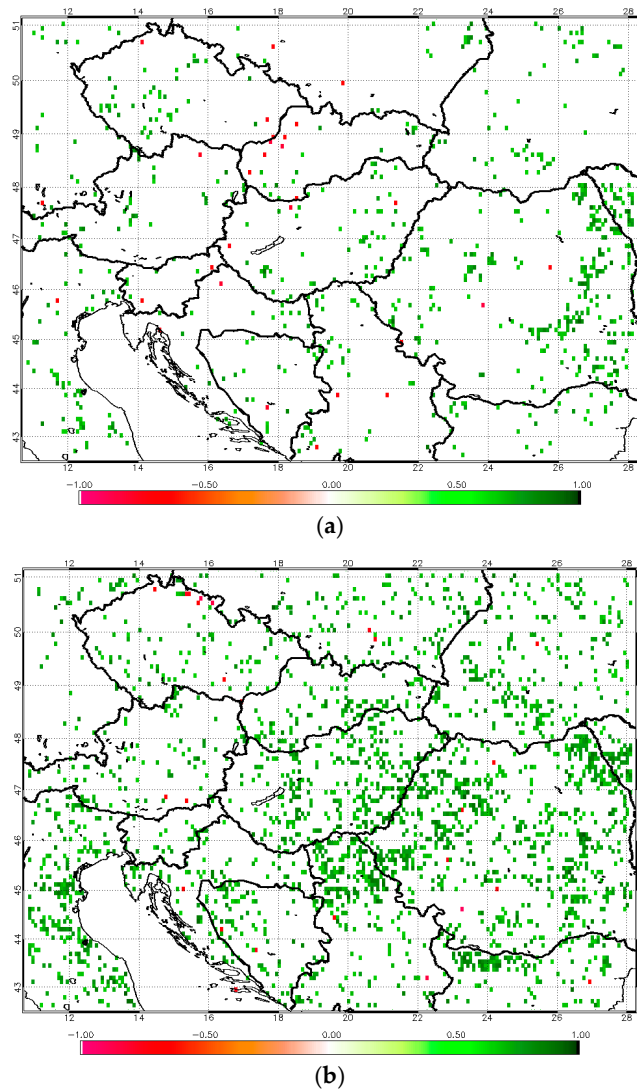


**Figure S8.** Maps of R between the EOS derived from (a) NDVI3go and the Terra/NDVI<sub>MODIS</sub> datasets and (b) NDVI3gh and the Terra/NDVI<sub>MODIS</sub> datasets, showing only the pixels with statistically significant R ( $p < 0.01$ ).

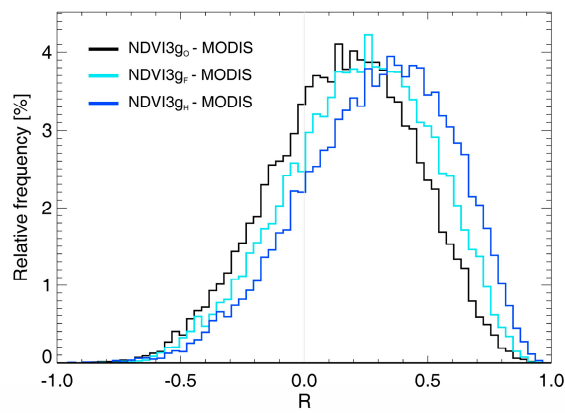


**Figure S9.** Frequency distribution of R values of EOS during the 2000–2013 time period for NDVI3go (black), NDVI3gr (light blue) and NDVI3gh (dark blue) datasets relative to the Terra NDVI<sub>MODIS</sub> dataset ( $n = 20191$ ).

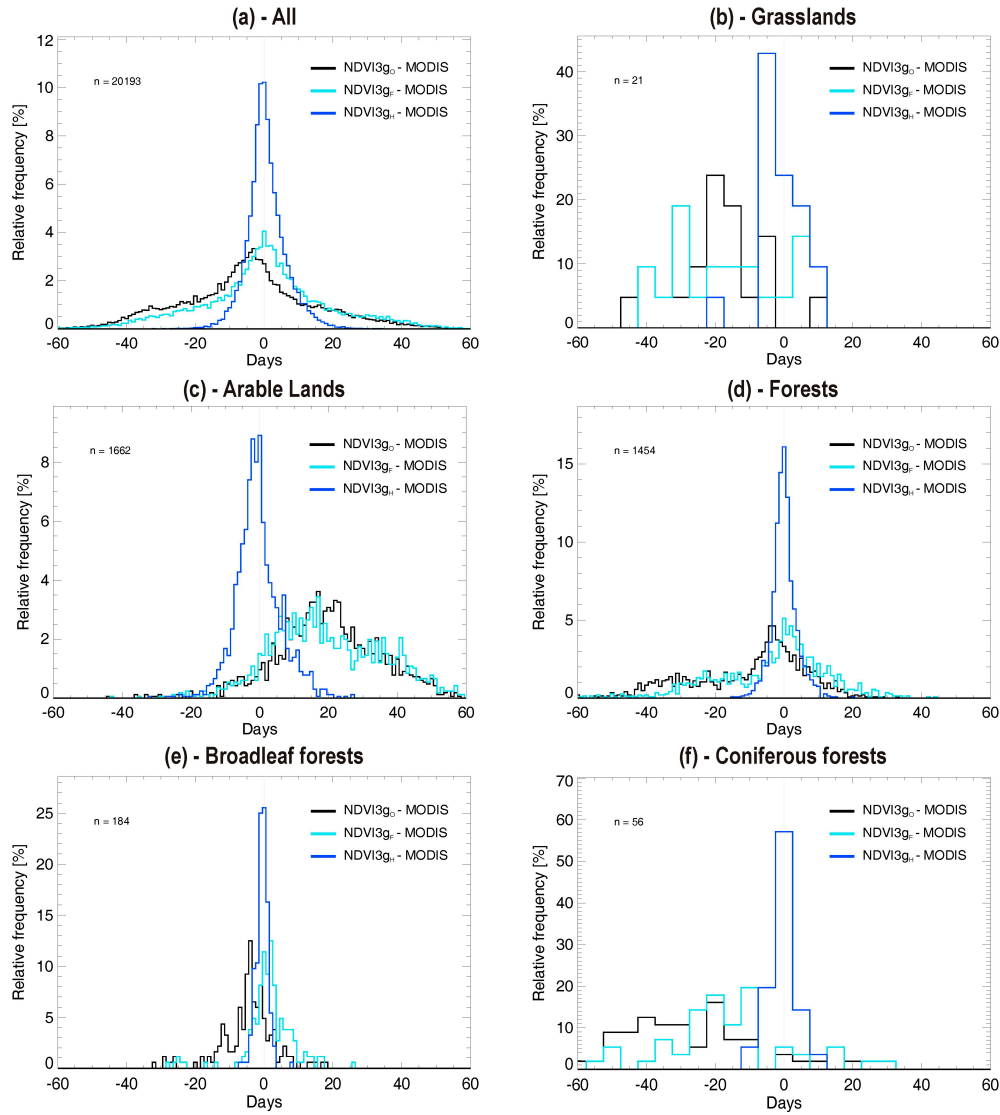


**Figure S10.** (a–f) Frequency distribution of bias of EOS during the 2000–2013 time period for NDVI3go (black), NDVI3g<sub>F</sub> (light blue) and NDVI3g<sub>H</sub> (dark blue) datasets relative to the Terra NDVI<sub>MODIS</sub> dataset for different land cover types. Positive bias means earlier EOS for MODIS.

**6. Additional Maps and Figures related to the Length of Season Comparison**

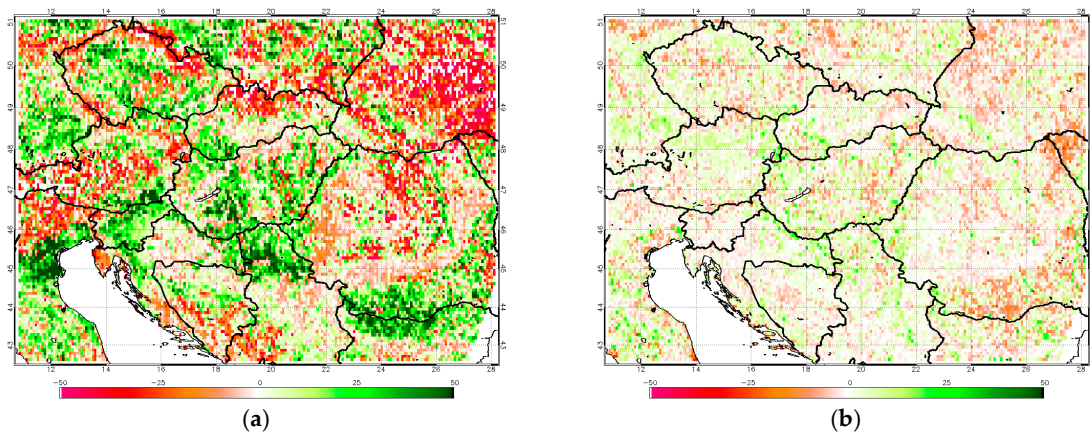


**Figure S11.** Maps of bias for the length of the season derived from (a) NDVI3go and the Terra/NDVI<sub>MODIS</sub> datasets and (b) NDVI3g<sub>H</sub> and the Terra/NDVI<sub>MODIS</sub> datasets (expressed in days).

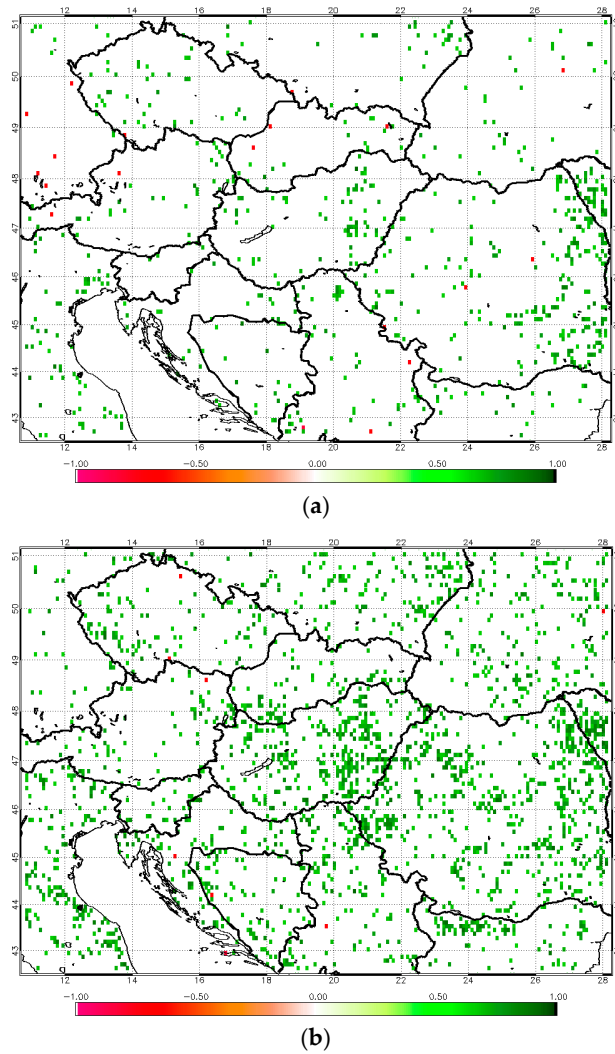


**Figure S12.** Maps of R between the length of the season derived from (a) NDVI3g<sub>0</sub> and the Terra/NDVI<sub>MODIS</sub> datasets and (b) NDVI3g<sub>H</sub> and the Terra/NDVI<sub>MODIS</sub> datasets, showing only the pixels with statistically significant R ( $p < 0.01$ ).

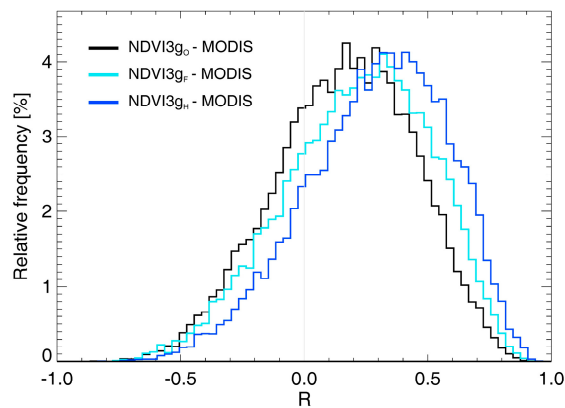


**Figure S13.** Frequency distribution of R values of length of the season during the 2000–2013 time period for NDVI3g<sub>0</sub> (black), NDVI3g<sub>F</sub> (light blue) and NDVI3g<sub>H</sub> (dark blue) datasets relative to the Terra NDVI<sub>MODIS</sub> dataset ( $n = 20191$ ).

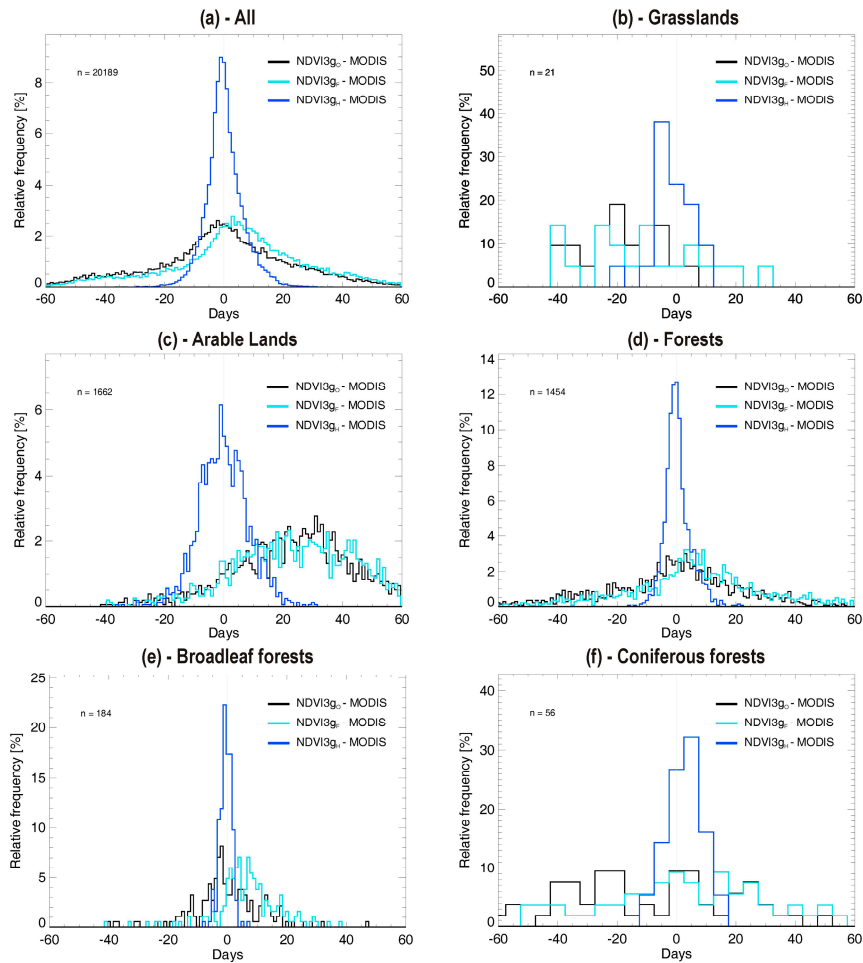


**Figure S14.** (a–f) Frequency distribution of length of the season bias during the 2000–2013 time period for NDVI3g<sub>0</sub> (black), NDVI3g<sub>F</sub> (light blue) and NDVI3g<sub>H</sub> (dark blue) datasets relative to the Terra NDVI<sub>MODIS</sub> dataset for different land cover types. Positive bias means shorter length of the season for MODIS.

**7. Additional Maps and Figures related to the Maximum NDVI Comparison**

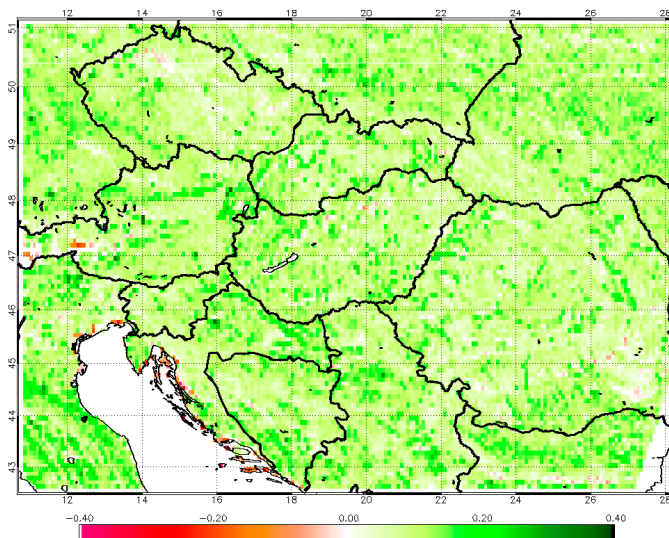


**Figure S15.** Map of bias of the maximum NDVI values during the 2000–2013 time period derived from NDVI3g<sub>0</sub> and the Terra/NDVI<sub>MODIS</sub> dataset.

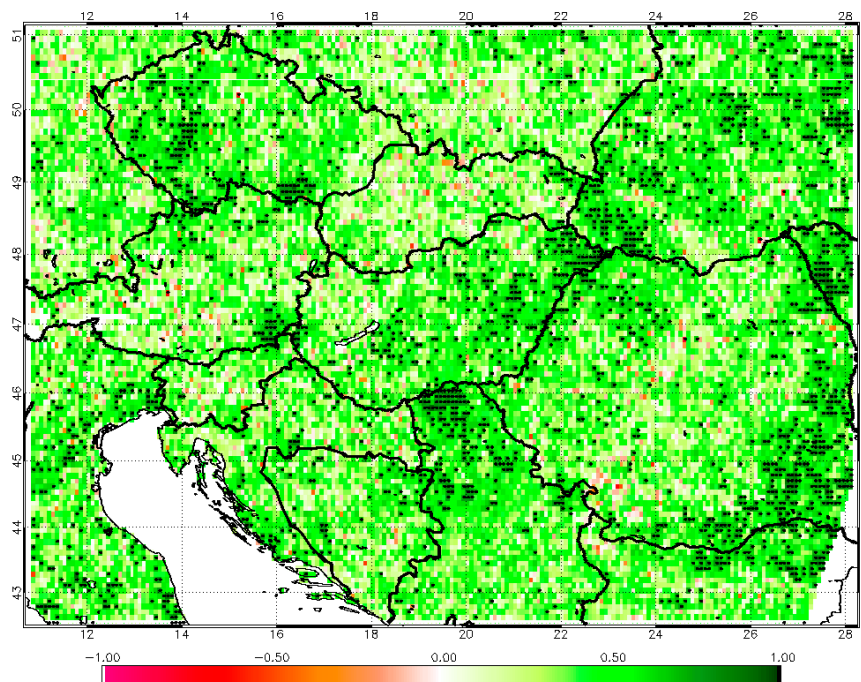


**Figure S16.** Map of R between the maximum NDVI values derived from NDVI3gH and the Terra/NDVIMODIS datasets, showing only the pixels with statistically significant R ( $p < 0.01$ ).

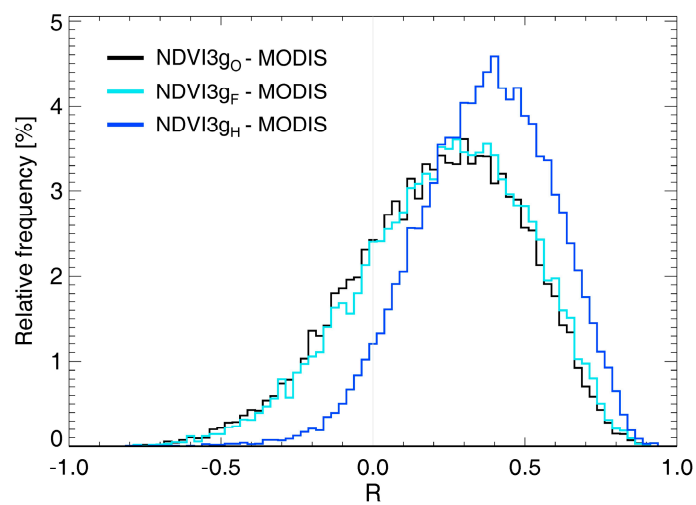


**Figure S17.** Frequency distribution of R of maximum NDVI bias between the NDVIMODIS and the NDVI3gO (black), NDVI3gF (light blue) and NDVI3gH datasets.

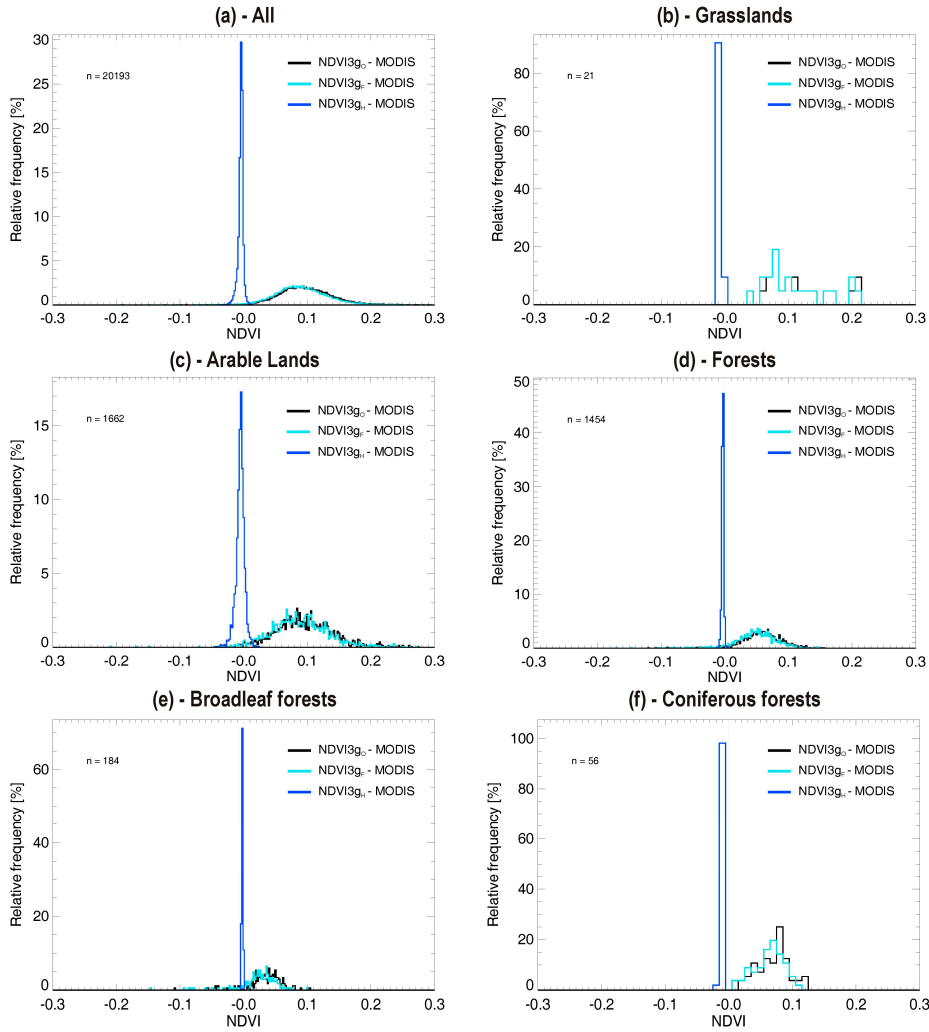


**Figure S18.** (a–f) Frequency distribution of bias of maximum NDVI during the 2000–2013 time period for NDVI3go (black), NDVI3gf (light blue) and NDVI3gH (dark blue) datasets relative to the Terra NDVI<sub>MODIS</sub> dataset for different land cover types. Positive bias means higher peak for NDVI3g.

**8. Additional Maps and Figures related to the Comparison of Timing of Maximum NDVI**

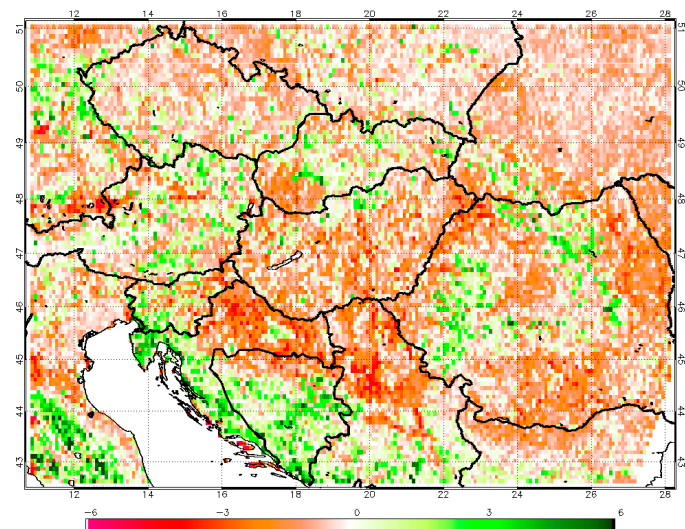


**Figure S19.** Map of bias of the time of the maximum NDVI values during the 2000–2013 time period derived from NDVI3go and the Terra/NDVI<sub>MODIS</sub> dataset.

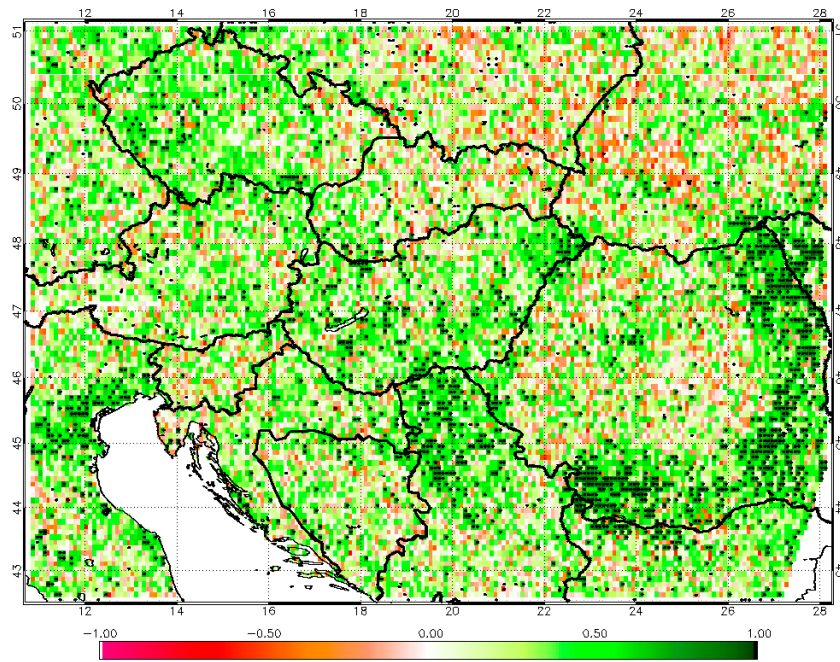


**Figure S20.** Map of R between the time of the maximum NDVI values derived from NDVI3g<sub>H</sub> and the NDVI<sub>MODIS</sub> datasets, indicating the pixels with  $p < 0.01$  with dots.

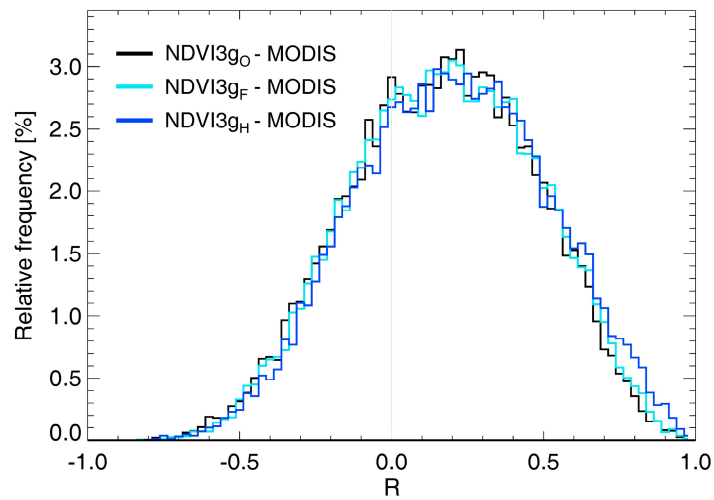


**Figure S21.** Frequency distribution of R of maximum NDVI timing between the NDVI<sub>MODIS</sub> and the NDVI3g<sub>O</sub> (black), NDVI3g<sub>F</sub> (light blue) and NDVI3g<sub>H</sub> datasets.

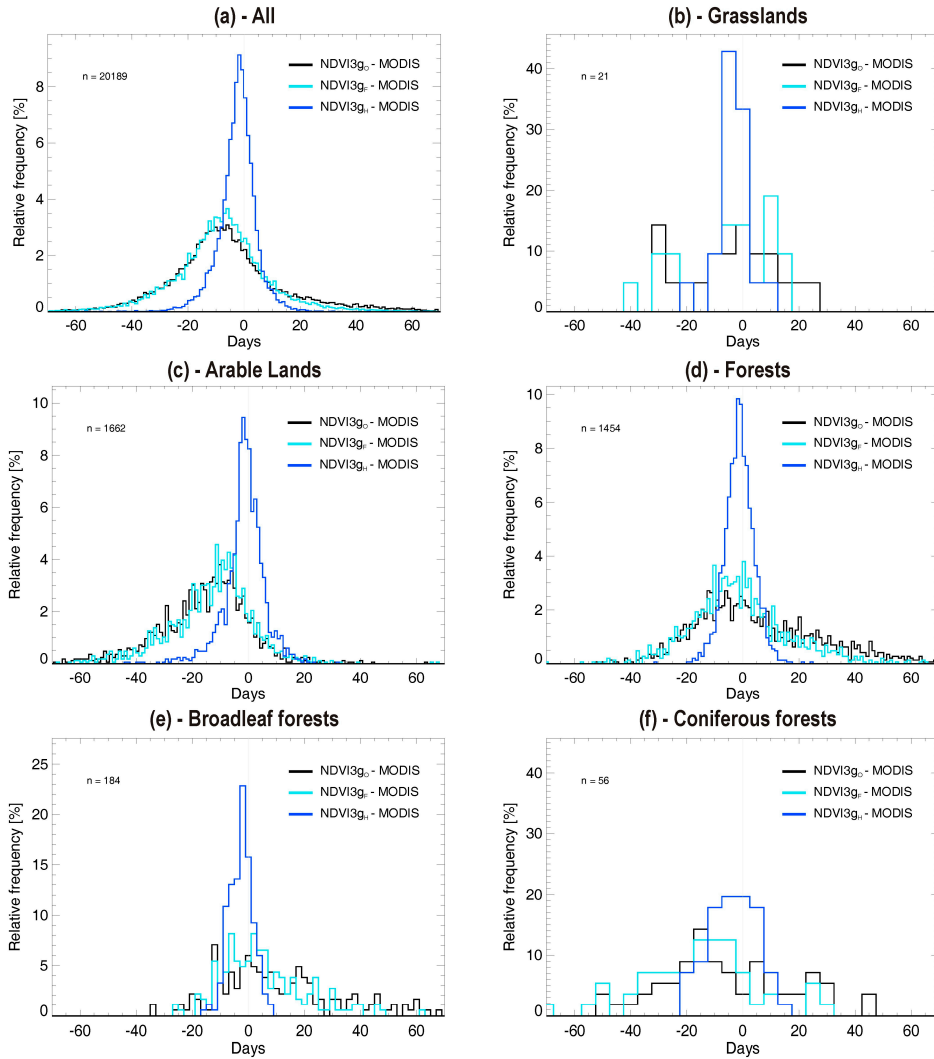


**Figure S22.** (a–f) Frequency distribution of timing of maximum NDVI during the 2000–2013 time period for NDVI3g<sub>O</sub> (black), NDVI3g<sub>F</sub> (light blue) and NDVI3g<sub>H</sub> (dark blue) datasets relative to the Terra NDVI<sub>MODIS</sub> dataset for different land cover types. Positive bias means earlier maximum NDVI for MODIS.

**9. Additional Maps and Figures related to the Comparison of NDVI Anomalies**

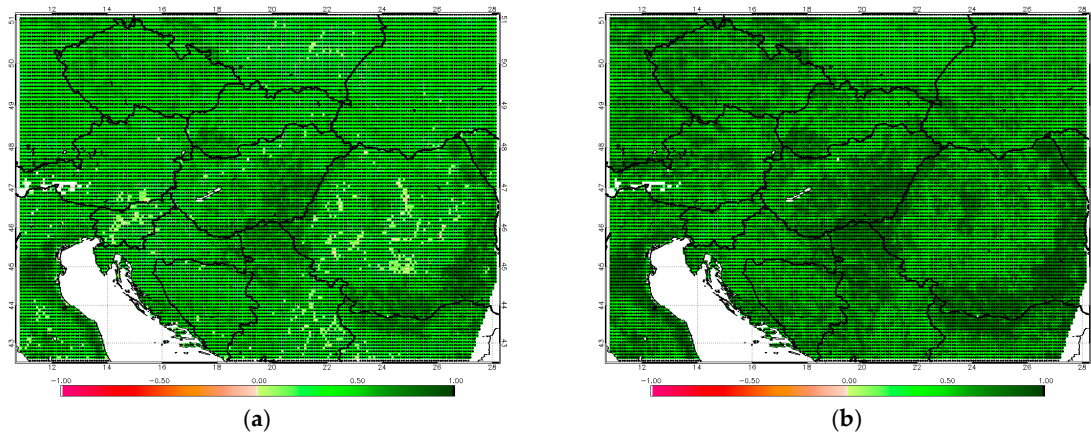


**Figure S23.** Maps of R values between the anomaly values derived from (a) the Terra/NDVI<sub>MODIS</sub> and NDVI3g<sub>O</sub> and (b) the Terra/NDVI<sub>MODIS</sub> and NDVI3g<sub>H</sub> datasets during the overlapping 14 years taking into account all 15-day periods, indicating the pixels with  $p < 0.01$  with dots inside.

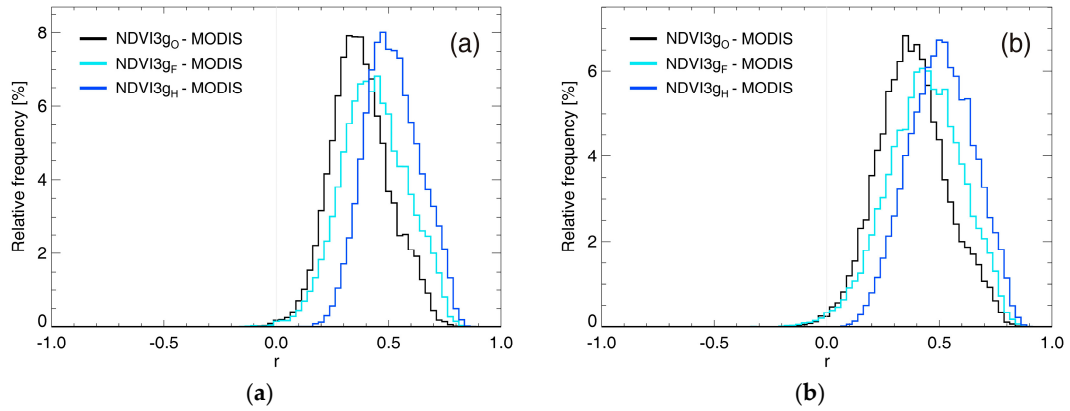


**Figure S24.** Distribution of the R values that characterize the relationship between the anomaly values of the  $NDVI_{MODIS}$  and  $NDVI3g_0$  (black),  $NDVI3g_F$  (light blue), and  $NDVI3g_H$  (dark blue) (a) for all 15-day periods and (b) only for the growing season (second half of April—first part of September;  $n = 20191$ ).

### 10. Additional Figures related to Quantifying the Relationship between Climate and NDVI Anomalies

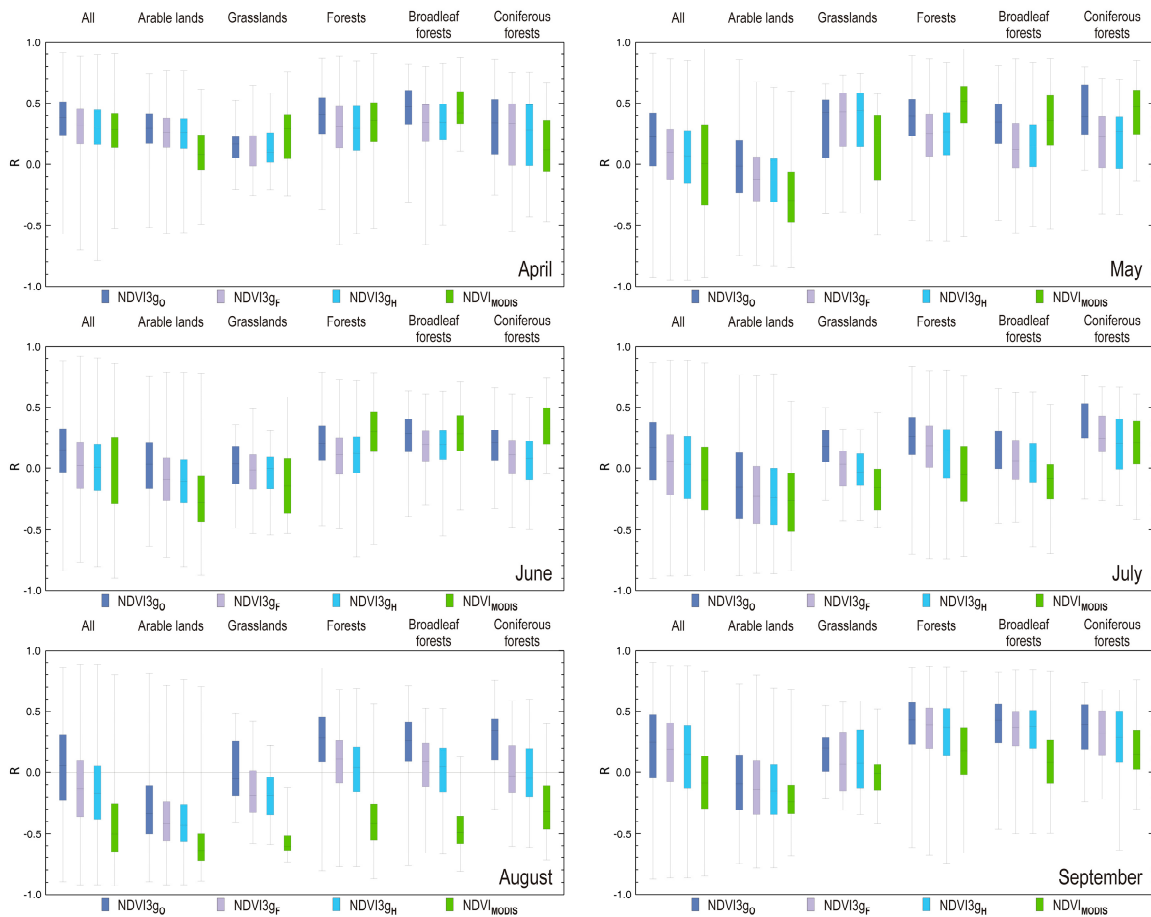


**Figure S25.** Box-whisker plots of the correlation coefficients between the temperature and NDVI anomaly for April, May, June, July, August and September derived from the  $NDVI3g_0$  (dark blue, first column in every LC group),  $NDVI3g_F$  (purple, second column in every LC group),  $NDVI3g_H$  (light blue, third column in every LC group) and  $NDVI_{MODIS}$  (green, fourth column in every group) datasets for all vegetated pixels of the domain, and for different land cover types. Box-whisker plots indicate maximum, upper quartile, median, lower quartile, and minimum values.

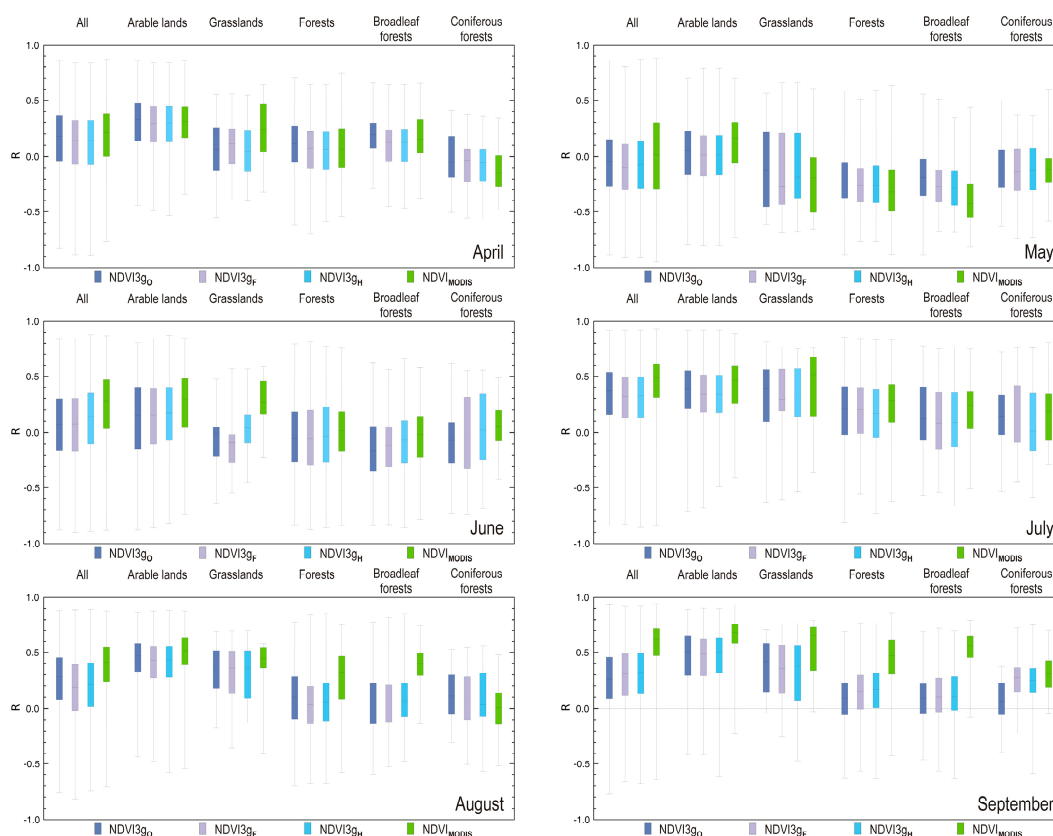


**Figure S26.** Box-whisker plots of the correlation coefficients between the precipitation anomaly of the previous month and NDVI anomaly for April, May, June, July, August and September derived from the NDVI3g<sub>0</sub> (dark blue, first column in every LC group), NDVI3g<sub>F</sub> (purple, second column in every LC group), NDVI3g<sub>H</sub> (light blue, third column in every LC group) and NDVI<sub>MODIS</sub> (green, fourth column in every group) datasets for all vegetated pixels of the domain, and for different land cover types. Box-whisker plots indicate maximum, upper quartile, median, lower quartile, and minimum values.

## 11. Additional Information on the Construction of NDVI3g

**Table S4.** Contributions of different AVHRR satellites to the NDVI3g dataset. Dates in the table denote the first day in the 15-day period of data acquisition.

Satellite	From Date	To Date	Full Year Coverage
NOAA-7	1 January 1982	16 February 1985	
NOAA-9	1 March 1985	16 October 1988	
NOAA-11	1 November 1988	16 August 1994	
NOAA-9	1 September 1994	1 January 1995	
NOAA-14	16 January 1995	16 October 2000	
NOAA-16	1 November 2000	16 December 2003	2001–2003
NOAA-17	1 January 2004	16 December 2008	2004–2008
NOAA-18	1 January 2009	16 December 2011	2009–2011
NOAA-19	1 January 2012	16 December 2013	2012–2013

